

RESEARCH ARTICLE

10.1002/2016JD025763

Key Points:

- Two MODIS products are compared with the collocated ground measurements from the ARM CAP-MBL campaign over Azores site
- Satellite and ground products agree reasonably well on cloud liquid water path and cloud optical thickness
- However, satellite-based cloud effective radius retrievals are about 1–3 microns larger than collocated ground-based retrievals

Correspondence to:

Z. Zhang,
zzbatmos@umbc.edu

Citation:

Zhang, Z., X. Dong, B. Xi, H. Song, P.-L. Ma, S. J. Ghan, S. Platnick, and P. Minnis (2017), Intercomparisons of marine boundary layer cloud properties from the ARM CAP-MBL campaign and two MODIS cloud products, *J. Geophys. Res. Atmos.*, 122, 2351–2365, doi:10.1002/2016JD025763.

Received 10 AUG 2016

Accepted 18 JAN 2017

Accepted article online 22 JAN 2017

Published online 17 FEB 2017

Intercomparisons of marine boundary layer cloud properties from the ARM CAP-MBL campaign and two MODIS cloud products

Zhibo Zhang^{1,2} , Xiquan Dong³ , Baike Xi⁴ , Hua Song² , Po-Lun Ma⁵ , Steven J. Ghan⁵ , Steven Platnick⁶ , and Patrick Minnis⁷ 

¹Physics Department, UMBC, Baltimore, Maryland, USA, ²Joint Center Joint Center for Earth Systems Technology, UMBC, Baltimore, Maryland, USA, ³Department of Hydrology and Atmospheric Sciences, University of Arizona, Tucson, Arizona, USA, ⁴Department of Atmospheric Sciences, University of North Dakota, Grand Forks, North Dakota, USA, ⁵Pacific Northwest National Laboratory, Richland, Washington, USA, ⁶NASA Goddard Space Flight Center, Greenbelt, Maryland, USA, ⁷NASA Langley Research Center, Hampton, Virginia, USA

Abstract From April 2009 to December 2010, the Department of Energy Atmospheric Radiation Measurement (ARM) program carried out an observational field campaign on Graciosa Island, targeting the marine boundary layer (MBL) clouds over the Azores region. In this paper, we present an intercomparison of the MBL cloud properties, namely, cloud liquid water path (LWP), cloud optical thickness (COT), and cloud-droplet effective radius (CER), among retrievals from the ARM mobile facility and two Moderate Resolution Imaging Spectroradiometer (MODIS) cloud products (Goddard Space Flight Center (GSFC)-MODIS and Clouds and Earth's Radiant Energy System-MODIS). A total of 63 daytime single-layer MBL cloud cases are selected for intercomparison. Comparison of collocated retrievals indicates that the two MODIS cloud products agree well on both COT and CER retrievals, with the correlation coefficient $R > 0.95$, despite their significant difference in spatial sampling. In both MODIS products, the CER retrievals based on the 2.1 μm band (CER_{2.1}) are significantly larger than those based on the 3.7 μm band (CER_{3.7}). The GSFC-MODIS cloud product is collocated and compared with ground-based ARM observations at several temporal-spatial scales. In general, the correlation increases with more precise collocation. For the 63 selected MBL cloud cases, the GSFC-MODIS LWP and COT retrievals agree reasonably well with the ground-based observations with no apparent bias and correlation coefficient R around 0.85 and 0.70, respectively. However, GSFC-MODIS CER_{3.7} and CER_{2.1} retrievals have a lower correlation ($R \sim 0.5$) with the ground-based retrievals. For the 63 selected cases, they are on average larger than ground observations by about 1.5 μm and 3.0 μm , respectively. Taking into account that the MODIS CER retrievals are only sensitive to cloud top reduces the bias only by 0.5 μm .

1. Introduction

Liquid-phase marine boundary layer (MBL) clouds cover approximately 20% of Earth's surface [Wood, 2012]. They are an important modulator of Earth's radiative energy budget [Klein and Hartmann, 1993]. A realistic and accurate representation of MBL clouds in general circulation models (GCM) is critical for understanding the global radiative energy budget, estimating aerosol effects on clouds, and projecting future climate change. Evaluating and improving GCM simulated MBL clouds requires accurate monitoring of MBL cloud microphysical and optical properties, as well as their association with environmental factors such as meteorological conditions and aerosol loading.

The need for such observations motivated the clouds, aerosol, and precipitation in the marine boundary layer (CAP-MBL) field campaign funded by the U.S. Department of Energy (DOE) Atmospheric Radiation Measurement (ARM) Program [Wood *et al.*, 2015]. In this campaign, the ARM Mobile Facility (AMF) was deployed to Graciosa Island (39.09°N, 28.03°W) for 21 months from April 2009 to December 2010. Graciosa Island is part of the Azores archipelago in the eastern Atlantic. It is subject to a wide range of different meteorological conditions, mostly involving marine stratus and stratocumulus clouds [Wood *et al.*, 2015; Dong *et al.*, 2014a]. Thus, it is an ideal location for observing MBL clouds and studying how they are influenced by environmental factors, such as aerosol loading and large-scale circulation pattern. The ARM AMF instruments provide a variety of cloud and aerosol observations, as well as related radiation fields and meteorological conditions. Recent studies have proven these observations to be a valuable data record for studying

aerosol and cloud interactions in an otherwise poorly sampled remote marine environment [Logan *et al.*, 2014; Dong *et al.*, 2014a, 2014b].

In addition to ground-based ARM observations, satellite sensors, such as the Moderate Resolution Imaging Spectroradiometer (MODIS) on board of NASA's Terra and Aqua satellites, are another important source of cloud property observations. Among many operational and research-level MODIS-based cloud property products that have been developed, two are best recognized and most widely used. The first one is the "MOD06" product developed and maintained by a science team at NASA Goddard Space Flight Center (GSFC) [Platnick *et al.*, 2003, 2016]. It will be referred to as the "GSFC-MODIS product" hereafter. The other one is developed by a science team at NASA Langley Research Center, as part of the Clouds and Earth's Radiant Energy System (CERES) project [Minnis *et al.*, 2011b], which will be referred to as the "CERES-MODIS product" hereafter. Both products have been used in previous studies for evaluating the cloud simulations in GCMs [e.g., Kay *et al.*, 2012; Pincus *et al.*, 2012; Dolinar *et al.*, 2014].

Ground-based ARM cloud observations and satellite-based MODIS cloud products are two important sources for cloud related studies and for GCM evaluations. It is important to assess and understand the potential differences between the two data sets. Recently, Xi *et al.* [2014] (referred to as Xi14 hereafter) compared the MBL cloud properties from the ARM's Graciosa site during CAP-MBL campaign to the CERES-MODIS cloud products for 63 daytime and 92 nighttime MODIS overpass cases. For collocation purposes, ground-based measurements are averaged over a 1 h window centered at the satellite overpass time, whereas the CERES-MODIS retrievals are averaged over a 30 km \times 30 km box centered at the Graciosa ARM site (referred to as "dL30km-dt60min" averaging scheme). The ground- and satellite-based measurements agree well on the cloud-top temperature of MBL clouds. However, they have significant differences in other cloud properties, including cloud LWP, COT, and CER. In particular, CERES-MODIS COT retrievals are on average smaller than their counterparts from ARM ground-based retrievals by about 4.1 or 30% ($R \sim 0.66$). One average, the CER retrievals from the CERES-MODIS CER_{2.1} and CER_{3.7} are larger than the ground-based retrievals by about 3.75 μm (30%) and 1.33 μm (10%), respectively ($R \sim 0.53$ and 0.49, respectively). The underestimated COT and overestimated CER in the CERES-MODIS product lead to error cancelation and a rather small LWP difference, generally within 12%, in comparison with ground-based retrievals ($R \sim 0.62$). Overall, it was found that the ground- and satellite-based cloud properties at the Graciosa site do not agree as well as their continental low cloud counterparts at ARM's SGP reported in Dong *et al.* [2008].

The differences between ground- and satellite-based cloud retrievals stem from two major sources. The first is the collocation uncertainty. Ground-based instruments make single-point observations, whereas satellite imagers like MODIS take instantaneous snapshots of a large area. In addition, all instruments have finite temporal and spatial resolutions. For example, the ground-based cloud retrievals have a nominal 5 min temporal resolution [Dong *et al.*, 1998; Xi *et al.*, 2014]. Xi14 is based on a dL30km-dt60min collocation scale. Ideally, a smaller temporal-spatial averaging window would allow a more precise match between ground- and satellite-based observations. However, the subsampling scheme used by the CERES-MODIS algorithm leads to an effective spatial resolution of approximately 2.8 km. As a result, it is difficult to reduce the spatial averaging domain to a much smaller size than 30 km while maintaining enough statistics. It remains unclear whether a more precise temporal-spatial collocation would lead to a better agreement between ground- and satellite-based observations.

The second source is due to the differences in retrieval methods and algorithms. For example, the MODIS CER retrieval algorithm is based on the cloud reflection of solar radiation in the shortwave infrared (SWIR) spectral region (e.g., 2.1 μm and 3.7 μm). Because of the cloud absorption, the SWIR band had only limited penetration depth into the cloud top and therefore the MODIS CER retrieval is only sensitive to the cloud microphysics in the upper part of the cloud [Platnick, 2000; Zhang and Platnick, 2011]. In contrast, the ground-based CER retrieval is based on the surface solar transmission measurement and therefore is a vertically averaged CER [Dong *et al.*, 1997; Dong and Mace, 2010]. Another example is that the ground-based cloud LWP is directly retrieved from microwave radiometer (MWR) observations, whereas MODIS LWP is a diagnostic variable derived from the COT and CER retrievals.

Xi14 analyzed the potential reasons for the differences in LWP, COT, and CER between ground-based retrievals and collocated CERES-MODIS retrievals, mainly from the perspective of differences in retrieval methods and algorithms. For example, they demonstrated in several cases that in comparison with the ground-based

CER profile retrievals, the CERES-MODIS CER retrievals based on different SWIR bands, i.e., 2.1 μm and 3.7 μm (hereafter referred to as CER_{2,1} and CER_{3,7}, respectively), are qualitatively aligned with theoretical expectations, i.e., CER_{2,1} penetrates deeper into the cloud than CER_{3,7}. Their investigation into the impacts of collocation uncertainty was limited by the subsampling scheme of the operational CERES-MODIS cloud retrieval algorithm. Although most MODIS bands have a nominal resolution of 1 km, the CERES-MODIS cloud retrieval algorithm only subsamples every fourth pixel and every other scan line of the 1 km MODIS measurements [Minnis *et al.*, 2011a]. As such, there is only a one eighth probability that the CERES-MODIS near-site pixel includes the site in its field of view. In some cases, the nearest CERES-MODIS pixel center may be as far as 10 km from the site. As a result, it remains unclear if the differences between ground-based and CERES-MODIS cloud properties are mainly due to differences in retrieval algorithm or collocation uncertainty.

This study is a follow-up to Xi14. In addition to the CERES-MODIS product, we introduce another MODIS product—the GSFC-MODIS cloud product—in the comparison with ground-based observations. As explained later, the GSFC-MODIS cloud product samples every 1 km MODIS observation, which enables a better temporal-spatial collocation with the ARM ground site. We first compare the pixel-level cloud properties, including cloud LWP, COT, and CER, from the two MODIS products with ground-based measurements for the 63 daytime overpass cases reported in Xi14. In addition, we also compare the monthly mean (i.e., level 3) MODIS cloud product with the aggregated ground-based measurements during the 19 month CAP-MBL campaign period.

One objective of this study is to better understand to what extent the ground- and satellite-based retrievals of MBL cloud properties agree with one another so that they can be used with greater confidence for evaluating and improving the MBL cloud simulations in GCMs. The rest of this paper is organized as follows. section 2 provides an overview of the ground-based and satellite-based cloud properties retrievals used for the inter-comparison. The comparison results for the 63 collocated MODIS overpass cases are presented and discussed in section 3.

2. Ground- and Satellite-Based Measurements and Retrievals

2.1. Ground-Based Cloud Properties From ARM CAP-MBL Campaign

2.1.1. Cloud LWP Retrievals From MWR

The ground-based cloud LWP product used in the intercomparison is derived from the MWR measurements at the ARM Graciosa site during the CAP-MBL campaign. The ARM MWR measures the downwelling brightness temperatures (BT) at surface at 23.8 and 31.4 GHz. Water vapor emission dominates the signal in the 23.8 GHz channel, whereas liquid water emission constitutes the primary portion of the signal at 31.4 GHz. Liljegren *et al.* [2001] developed a statistical retrieval method to retrieve both LWP and total precipitable water vapor (PWV) simultaneously from the dual frequency BT measurements. This algorithm is simple, computationally fast and has been adopted as the operational LWP and PWV retrieval algorithm for ARM MWR. Its main limitation is that the retrieval parameters required in this algorithm are based on a statistical fitting of the measured BT to the simulated BT from radiative transfer model. As a result, the instantaneous retrievals from this algorithm may be subject to significant uncertainties, approximately 25 g/m² for LWP and 0.5 mm for PWV (<http://www.arm.gov/instruments/mwr>).

Instantaneous MWR retrievals are known to be noisy due to broken clouds and/or retrieval uncertainties. For better data quality, the instantaneous MWR LWP retrievals (~20 s frequency) are aggregated to 5 min intervals. Cloud fractions and boundary retrievals from ARM's active sensors, including ceilometer and cloud profiling radar, are used during the aggregation to screen out clear sky and overlapping cloud conditions. Namely, MWR LWP retrievals are aggregated only when active sensors detect overcast single-layer low clouds within a 5 minute period. Therefore, the MWR LWP retrievals for the 63 selected cases used in the intercomparison are averaged *in-cloud* LWP with a 5 min frequency.

2.1.2. CER and COT Retrievals Based On Dong *et al.* [1998] Parameterization Scheme

The ground-based cloud CER and COT property retrievals for MBL clouds are based on the algorithm described in Dong *et al.* [1997, 1998]. The inputs to the algorithm include the abovementioned aggregated 5 minute LWP retrieval from the MWR and the downwelling solar flux at the surface from ground pyranometer measurements. Dong *et al.* [1998] developed a simple CER parameterization scheme, which has

proven to provide equally accurate CER retrievals as the interactive scheme in *Dong et al.* [1997]. The scheme is as follows:

$$\begin{aligned} \overline{\text{CER}}(\text{LWP}, \gamma) = & -2.07 + 2.49\text{LWP} + 10.25\gamma - 0.25\mu_0, \\ & + 20.28\text{LWP} \cdot \gamma - 3.14\text{LWP} \cdot \mu_0 \end{aligned} \quad (1)$$

where LWP is from the MWR, μ_0 is the cosine of solar zenith angle and $\gamma = F_{\text{cloudy}}^{\downarrow} / F_{\text{clear}}^{\downarrow}$ is the ratio of measured cloudy-sky downwelling solar flux ($F_{\text{cloudy}}^{\downarrow}$) to the expected clear-sky downwelling solar flux ($F_{\text{clear}}^{\downarrow}$) when there were no clouds [Long and Ackerman, 2000]. The upper bar in $\overline{\text{CER}}$ indicates that the retrieval is based on the vertically homogeneous cloud assumption and $\overline{\text{CER}}$ can be considered as an effective vertical average of the CER profile. A new algorithm developed by *Dong and Mace* [2010] and *Dong et al.* [2014b] to retrieve the profiles of CER and LWC is overviewed in the next section.

2.1.3. CER and LWC Profile Retrievals

As explained above, the retrievals based on *Dong et al.* [1998] can be considered as a vertically averaged CER. *Dong and Mace* [2010] developed a new retrieval scheme that combines the radar reflectivity profile ($Z(h)$) from the K band (35 GHz) millimeter wavelength radar (MMCR), LWP from MWR, and pyranometer γ measurements to retrieve the vertical profile of CER and liquid water content (LWC) of MBL clouds. On the basis of the lognormal particle size distribution (PSD) assumption and the analytical relations between radar reflectivity and PSD, *Dong and Mace* [2010] related the vertical profile of CER to the $Z(h)$ profile from MMCR and the vertically averaged CER based on *Dong et al.* [1998] as follows:

$$\text{CER}(h) = \overline{\text{CER}} \cdot \left[\frac{\Delta H \cdot Z^{1/2}(h)}{\Delta h \sum_{\text{base}}^{\text{top}} Z^{1/2}(h)} \right]^{1/3}, \quad (2)$$

where $\overline{\text{CER}}$ is from the *Dong et al.* [1998] parameterization scheme in equation (1), ΔH is the physical thickness of the MBL cloud, and Δh is the MMCR range gate spacing. Once $\text{CER}(h)$ is known from equation (2), other key cloud properties such as the LWC profile can be easily derived from $\text{CER}(h)$ and the assumed PSD.

2.2. GSFC-MODIS and CERES-MODIS Cloud Products

In this study, we use the latest Edition-4 CERES-MODIS product [Minnis *et al.*, 2011b, 2011c] and the collection 6 GSFC-MODIS cloud product [Platnick *et al.*, 2016].

Both MODIS cloud products use the so-called bispectral method to simultaneously retrieve COT and CER from cloud reflectance measurements in two spectral bands [Nakajima *et al.*, 1990]. One measurement is usually made in the visible or near-infrared spectral region (e.g., 0.64 μm or 0.86 μm), where water absorption is negligible and therefore cloud reflection generally increases with COT. The other measurement is usually in the shortwave infrared (SWIR) spectral region (e.g., 2.1 or 3.7 μm), where water droplets are moderately absorptive and cloud reflectance generally decreases with increasing CER for optically thick clouds. Once the COT and CER are determined using the bispectral method, the LWP can be derived from the equation $\text{LWP} = 2/3\rho_w\text{COT} \cdot \text{CER}$.

MODIS has three SWIR bands centered at 1.6, 2.1, and 3.7 μm , respectively, which can all be used for CER retrieval in the bispectral method. Both MODIS cloud products report the CER retrievals based on the 2.1 μm and 3.7 μm retrievals (i.e., $\text{CER}_{2.1}$ and $\text{CER}_{3.7}$). In addition, the GSFC-MODIS also reports the $\text{CER}_{1.6}$. A number of recent studies found significant differences between $\text{CER}_{2.1}$ and $\text{CER}_{3.7}$ in the GSFC-MODIS and CERES-MODIS products for MBL clouds [Nakajima *et al.*, 2010; Painemal and Zuidema, 2011; Zhang and Platnick, 2011; Zhang *et al.*, 2012]. Subpixel cloud inhomogeneity is an important cause of this spectral difference [Zhang and Platnick, 2011; Zhang *et al.*, 2012]. Note that when $\text{CER}_{2.1}$ and $\text{CER}_{3.7}$ are used to derive the LWP, the retrievals are referred to as $\text{LWP}_{2.1}$ and $\text{LWP}_{3.7}$, respectively.

A major difference between the two MODIS cloud products is in their spatial sampling scheme. The CERES-MODIS product is developed mainly to facilitate the CERES measurements of the top-of-atmosphere (TOA) radiation [Minnis *et al.*, 2004, 2011b]. The CERES scanners on Terra and Aqua have a nadir spatial resolution of ~ 20 km. They rely on the high-resolution MODIS observations to identify the atmospheric and surface components within the CERES field of view so that the measured CERES broadband radiances can be

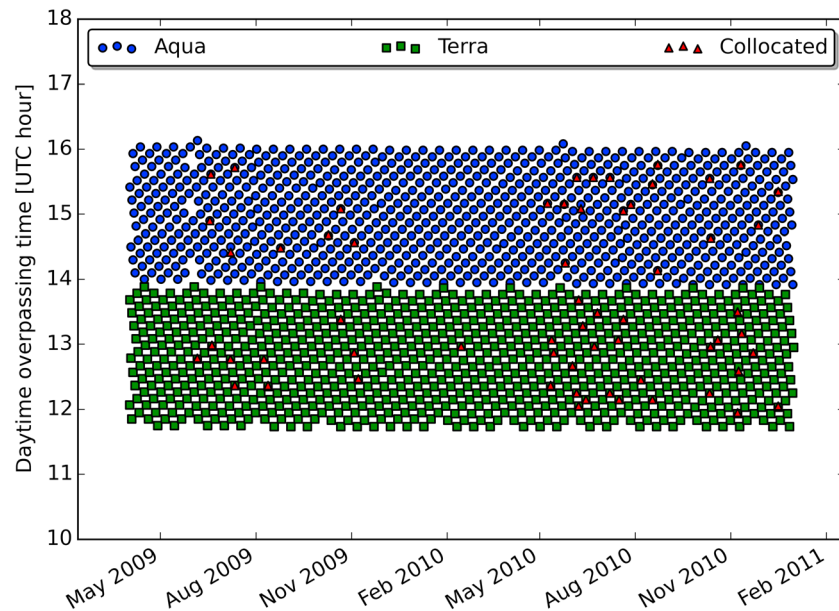


Figure 1. MODIS swath overpass times for Graciosa Island ($39^{\circ} 5' 28''$ N, $28^{\circ} 1' 45''$ W) during the CAP-MBL campaign. Blue dots (Aqua) and green squares (Terra) indicate MODIS swath overpass times. Red triangles mark the 63 daytime collocated cases in Xi *et al.* [2014].

converted into fluxes [Loeb *et al.*, 2005]. In order to minimize the processing time, the CERES-MODIS retrieval algorithm subsamples every fourth pixel and every other scan line of the 1 km MODIS measurements. As a result, the CERES-MODIS cloud product has an effective spatial resolution of 2.8 km. Thus, there are approximately 50 CERES-MODIS cloud retrievals in a 20 km CERES footprint. The operational level 2 CERES-MODIS cloud retrieval product is released together with the CERES TOA radiation measurements in the CERES-Single Scanner Footprint (SSF) product (https://eosweb.larc.nasa.gov/project/ceres/ssf_table). For each 20 km CERES footprint in the data, the corresponding cloud property statistics, such as mean and standard deviation, are reported based on the ~ 50 subsampled MODIS retrievals. For CERES Edition 4, the individual subsampled CERES-MODIS pixel retrievals are also archived for additional analyses. The pixel retrievals for a $30 \text{ km} \times 30 \text{ km}$ box centered on the ARM site were used in Xi14.

In contrast to the CERES-MODIS subsampling scheme, in the latest collection 6 of the GSFC-MODIS cloud product, the CER and COT retrievals are attempted for every possible 1 km cloudy pixel. The retrieval results for overcast and potentially partly cloudy pixels are reported separately in the product to reflect their difference in terms of retrieval quality.

3. Intercomparison Results for Xi14 Cases

The polar orbit and the wide cross-track swatch (2330 km) enable each MODIS to sample the Graciosa site on daily basis (once most days and some days twice). Figure 1, plots the Aqua- and Terra-MODIS swath overpass times for Graciosa Island during the CAP-MBL campaign period. The overpass time for Aqua is mostly between 14:00 and 16:00 UTC, while it is mostly between 12:00 and 14:00 UTC for Terra. During the whole CAP-MBL campaign period, each MODIS made over 830 daytime observations over Graciosa Island. However, most of these overpasses are not ideal for intercomparison purpose because the area is either cloud free or not covered by single-layer MBL clouds (e.g., covered by ice cloud or overlapping clouds). Indeed, Xi14 only found 63 overpassing cases, in which the Graciosa Island region—a $30 \text{ km} \times 30 \text{ km}$ box centered at ARM AMF site—is covered by single-layered overcast MBL clouds according to the CERES-MODIS cloud product.

It should be mentioned that when using the 1 km GSFC-MODIS cloud mask product to derive the cloud fraction in the same region, a number of scenes in the 63 cases are actually not overcast (cloud fractions as low as 60%), but the ARM MMCR and lidar observations show a continuous cloud layer. This difference

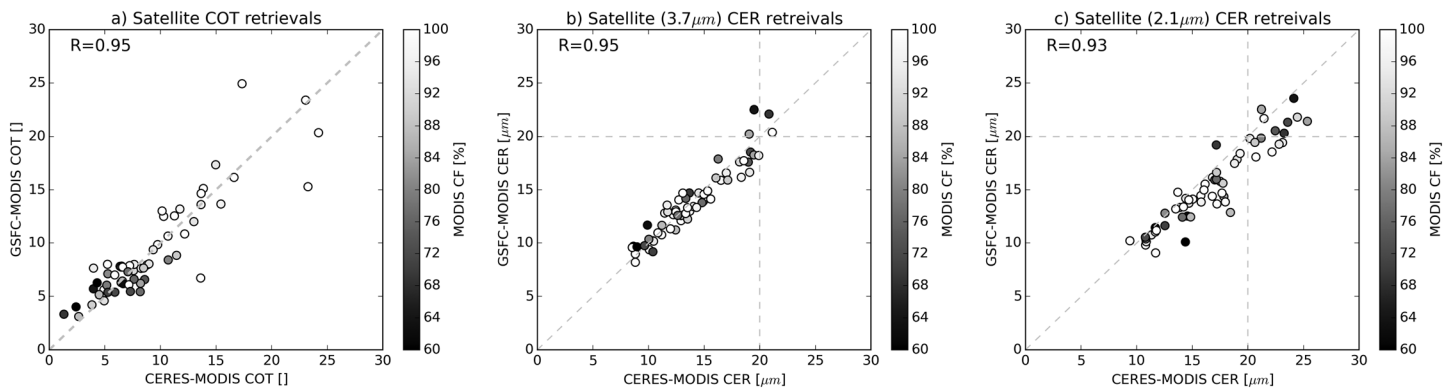


Figure 2. Comparison of (a) COT, (b) CER_{2.1}, and (c) CER_{3.7} of MBL clouds between collocated the CERES-MODIS and GSFC-MODIS products for the 63 selected cases in Xi14.

may be due to the subsampling scheme of the CERES-MODIS cloud product, leading to an overestimation of cloud fraction in some mostly cloudy scenes when the cloud-free pixels may not be sampled. Nevertheless, the intercomparison results indicate that the difference of cloud fraction between the two MODIS cloud products has little impact on the comparison. We start our intercomparison with these cases because they are relatively simple and also because our results are directly comparable with those reported in Xi14.

3.1. Comparison of GSFC- and CERES-MODIS Products

Before exploring the differences between ground-based retrievals with the MODIS cloud results, we first compare the two MODIS cloud products. For collocation, we first identify in the level 2 CERES-SSF product the CERES footprint closest to the ARM's AMF site on the Graciosa Island. Then, we found all the 1 km pixels of the GSFC-MODIS cloud retrievals within the 20 km CERES footprint as identified in the previous step. Finally, we averaged the GSFC-MODIS cloud retrievals from all the cloudy pixels within the CERES footprint and compared them with the averaged CERES-MODIS values reported in the CERES-SSF product that are based on the ~50 subsampled pixels.

Figure 2 shows the comparisons of COT, CER_{3.7} and CER_{2.1} between the collocated CERES-MODIS and GSFC-MODIS for the 63 Xi14 cases. The gray scale of the dots corresponds to the cloud fraction over the 30 km × 30 km box centered at ARM AMF site according to the GSFC-MODIS 1 km cloud mask product. Evidently, the two products are in close agreement, regardless of the cloud fraction. The correlation coefficients for COT and CER_{3.7} are both 0.95, and there is no apparent systematic bias between the two products. This is very encouraging even though the comparison is based on limited cases.

What is a little surprising is that the CER_{2.1} retrievals from the CERES-MODIS product are systematically larger than their GSFC-MODIS counterparts in Figure 2c, although the correlation efficient remains as high as 0.93. This difference appears to be greater for larger CER values and could be partially due to small differences in the C5 and C6 Terra 2.1 μm calibrations used by the CERES-MODIS and GSFC-MODIS analyses. Because of the nonlinear relationship between reflectance and CER_{2.1}, a given fractional change in the reflectance, equivalent to a change in the calibration gain, will cause a much larger change in CER_{2.1} for large droplets than for small droplets. Differences in the treatment of atmospheric absorption or in the modeling of the top-of-atmosphere reflectances could also account for the size-dependent CER_{2.1} difference between CERES-MODIS and GSFC-MODIS. This result implies that there is a larger difference between CER_{3.7} and CER_{2.1} in the CERES-MODIS product than in the GSFC-MODIS product, which is confirmed in Figure 3. In the GSFC-MODIS product (Figure 3a), the CER_{2.1} is larger than CER_{3.7} for all but one case. The results in Figure 3b indicate that the CERES-MODIS product has the same issue. The magnitude of the spectral difference is even larger.

As explained in several previous studies, subpixel cloud inhomogeneity (SPI) is an important cause of the spectral difference between CER_{3.7} and CER_{2.1} [e.g., Zhang and Platnick, 2011; Painemal et al., 2012; Zhang et al., 2012]. To examine the dependence of the spectral difference between CER_{3.7} and CER_{2.1} on SPI, we colored each case in Figure 3 based on the mean SPI index of the MBL cloud pixels in each case from the GSFC-MODIS product.

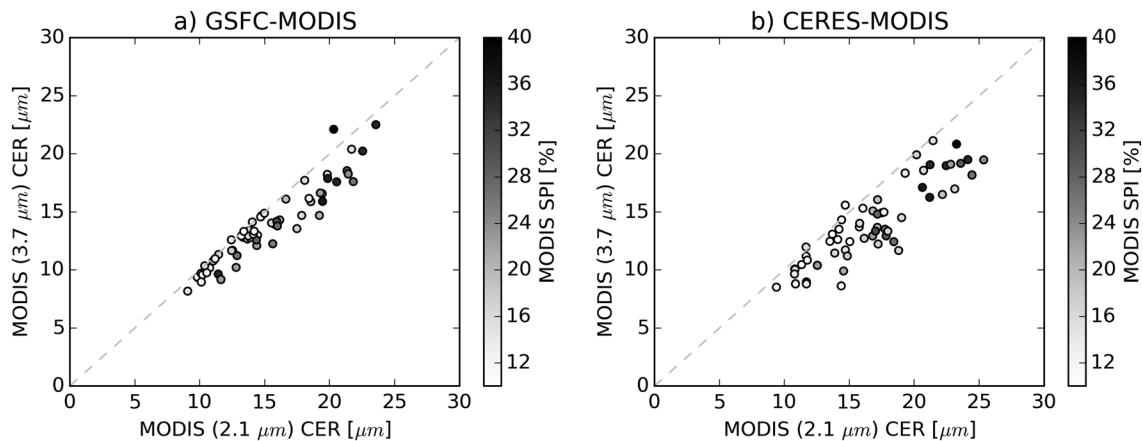


Figure 3. Comparison between $CER_{2.1}$ and $CER_{3.7}$ in (a) GSFC-MODIS and (b) CERES-MODIS cloud products for the 63 selected cases.

This SPI index product is derived from the 250 m subpixel variance of cloud reflectance, which is close to zero for highly homogeneous cloud and up to about 1.0 for highly inhomogeneous clouds. In general, we see that the cases with larger SPI (darker dots) tend to have larger spectral difference between $CER_{2.1}$ and $CER_{3.7}$ than those with more homogenous cases with smaller SPI (lighter dots). Similar results were found by *Painemal et al.* [2013] using the 2.8 km CERES-MODIS data to estimate horizontal homogeneity.

The dependence on SPI index is further examined in Figure 4. The background color map of the figure corresponds to the mean $CER_{2.1}-CER_{3.7}$ at each combination of SPI index and $CER_{2.1}$ derived from the total population of GSFC-MODIS pixels from all 63 Xi14 cases. The dotted contour lines correspond to the relative sampling rate (the center contour line has the largest sampling rate). Each dot in the figure corresponds to one of the 63 Xi14 cases. The location of the dots on x and y axis corresponds to the mean value of SPI index and $CER_{2.1}$ of each case, respectively. The color of each dot corresponds to the mean

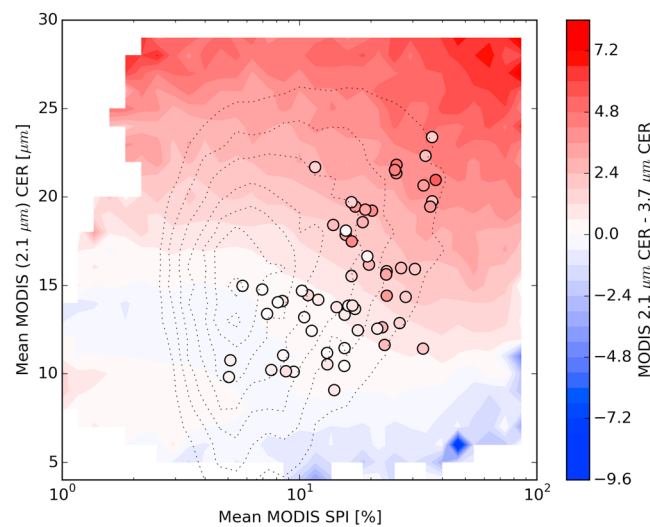


Figure 4. A composite plot of $CER_{2.1}-CER_{3.7}$ as a joint function of MODIS subpixel inhomogeneity index (SPI) and $CER_{2.1}$. The background color map corresponds to the mean $CER_{2.1}-CER_{3.7}$ at each pair of SPI index and $CER_{2.1}$ derived from the total population of GSFC-MODIS pixels for all 63 cases. The dotted contour lines correspond to the sampling rate. Each dot in the figure corresponds to one of the 63 cases. The location of the dots on x and y axis corresponds to the mean value of SPI index and $CER_{2.1}$ of each case, respectively. The color of each dot corresponds to the mean $CER_{2.1}-CER_{3.7}$ of each case.

$CER_{2.1}-CER_{3.7}$ value of each case. The background color pattern in Figure 4 reveals a rather complicated dependence of $CER_{2.1}-CER_{3.7}$ on both SPI index and $CER_{2.1}$, which is a manifestation of multiple mechanisms operating at the same time and entangled with one another [Zhang and Platnick, 2011; Zhang et al., 2012]. Nonetheless, a general pattern in Figure 4 is that, in the region with relatively high sampling rate, the $CER_{2.1}-CER_{3.7}$ difference tends to increase with increasing SPI index as a result of the aforementioned Plane-Parallel Homogeneous Bias (PPHB). It is encouraging to see the color of the dots, which is based on the mean value of $CER_{2.1}-CER_{3.7}$ in each case, is in general agreement of the background color based on the total population of pixels from all 63 cases. Overall, the results in Figures 3 and 4 suggest that the PPHB plays an important role in causing the size difference between $CER_{2.1}$ and $CER_{3.7}$ for the Xi14 cases.

In summary, the COT and CER_{3,7} retrievals from the CERES-MODIS product agree well with their GSFC-MODIS counterparts for the 63 MBL cloud cases studied here. In both products, the CER_{2,1} retrievals are systematically larger than the CER_{3,7} retrievals. This spectral difference is more severe in the CERES-MODIS product than in the GSFC-MODIS product. As a result, the CERES-MODIS CER_{2,1} retrievals are systematically larger than those from GSFC-MODIS. The PPHB is likely to be an important reason causing the spectral difference between CER_{2,1} and CER_{3,7}.

3.2. Comparisons of ARM Ground-Based Retrievals With the GSFC-MODIS Product

In this section, we focus on the comparison between ground-based cloud retrievals with the GSFC-MODIS product. We do *not* include CERES-MODIS product in the comparison for two reasons. First, as shown in the last section the two MODIS cloud products are in excellent agreement, which implied that whatever lessons are learned from the comparison about the GSFC-MODIS product should also apply to the CERES-MODIS product. Second, as mentioned in section 2.2, because of the subsampling scheme of CERES-MODIS retrieval algorithm and how the retrieval results are organized and reported in the CERES-SSF product, it is difficult to make precise collocation between the CERES-MODIS retrievals and ground measurements. For this reason Xi14 used the dL30km-dt60min averaging scheme. Because the GSFC-MODIS algorithm attempts a retrieval for every 1 km pixel, it has a spatial sampling rate about 8 times higher than the CERES-MODIS cloud product. This provides us an opportunity to investigate if closer temporal-spatial matching yields better agreement between ground- and satellite-based cloud retrievals. For this purpose, we developed a total of nine matching conditions based on the cross combinations of three spatial averaging dimensions $dL = 30, 20, \text{ and } 10 \text{ km}$ and three temporal averaging windows $dt = 60, 30, \text{ and } 10 \text{ min}$. Therefore, we focus on the GSFC-MODIS product in the comparisons that follow.

Figure 5 shows the results from LWP comparison. As shown in Figures 5a and 5b when we use the dL30km-dt60min averaging scheme, the correlation coefficient between the ground-based MWR LWP retrievals and the corresponding GSFC-MODIS LWP retrievals product is about 0.62 for the 63 Xi14 cases. This value is identical to that reported in Xi14 based on the CERES-MODIS product (see their Figure 8c), which is expected, given the excellent agreement between the two MODIS products. To explore the sensitivity to matching conditions, we progressively reduced the temporal-spatial averaging window in nine sensitivity tests. The resulting correlation coefficients from these tests are listed in Table 1. Apparently, the correlation between ground- and satellite-based LWP keeps increasing with decreasing temporal-spatial averaging window, from the lowest value of about 0.62 for dL30km-dt60min (Figures 5a and 5b) to the highest value of about 0.85 for dL10km-dt10min (Figures 5c and 5d). This is aligned with the expectation that closer collocation leads to better agreement between ground- and satellite-based retrievals. The small arrow in Figure 5 marks a prominent and interesting case that attests the importance of close collocation for matching ground- and satellite-based observations. This case was observed on 14 May 2010 around 12:50 UTC. Figure 6 shows the RGB image of this case from the Terra-MODIS. Zooming in on Graciosa Island, one can find that the island is covered by thick MBL clouds, while the surrounding region is either clear or covered by thinner clouds. While this could be due to island effects or simply a coincidence, it is evident that a dL30km averaging range would include a large fraction of thin clouds around the island. As a result the mean satellite-based LWP in Figures 5a and 5b is quite low, only $\sim 40 \text{ g/m}^2$, while the ground-based LWP is almost 8 times larger at $\sim 320 \text{ g/m}^2$. Reducing the temporal-spatial averaging window to dL10km-dt10min (Figures 5c and 5d) significantly increases the satellite-based LWP and also reduces the ground-based LWP, leading to a much closer agreement.

The presence of precipitation in MBL clouds poses challenges to both MWR and MODIS LWP retrievals. The current operational MWR retrieval algorithm considers only the absorption effect of cloud water and ignores the scattering effect. This assumption can be problematic for drizzling MBL clouds, because the drizzle drops are large enough to have significant scattering in MWR wavelength [Liljegren *et al.*, 2001]. The difficulties in retrieving cloud water when drizzle is present using microwave sensors are discussed in Lebsack and L'Ecuyer [2011] and Lebsack *et al.* [2011]. For MODIS retrieval, the changes of vertical structure and microphysics (e.g., bimodal PSD) caused by the warm rain process can make the properties of drizzling MBL clouds deviate from the fundamental assumptions made in the operational MODIS algorithm and results in significant uncertainty [Seethala and Horváth, 2010; Lebsack and Su, 2014; Miller *et al.*, 2016]. In Figure 5, we marked each case with a gray scale according to the fraction of precipitation during the temporal averaging window

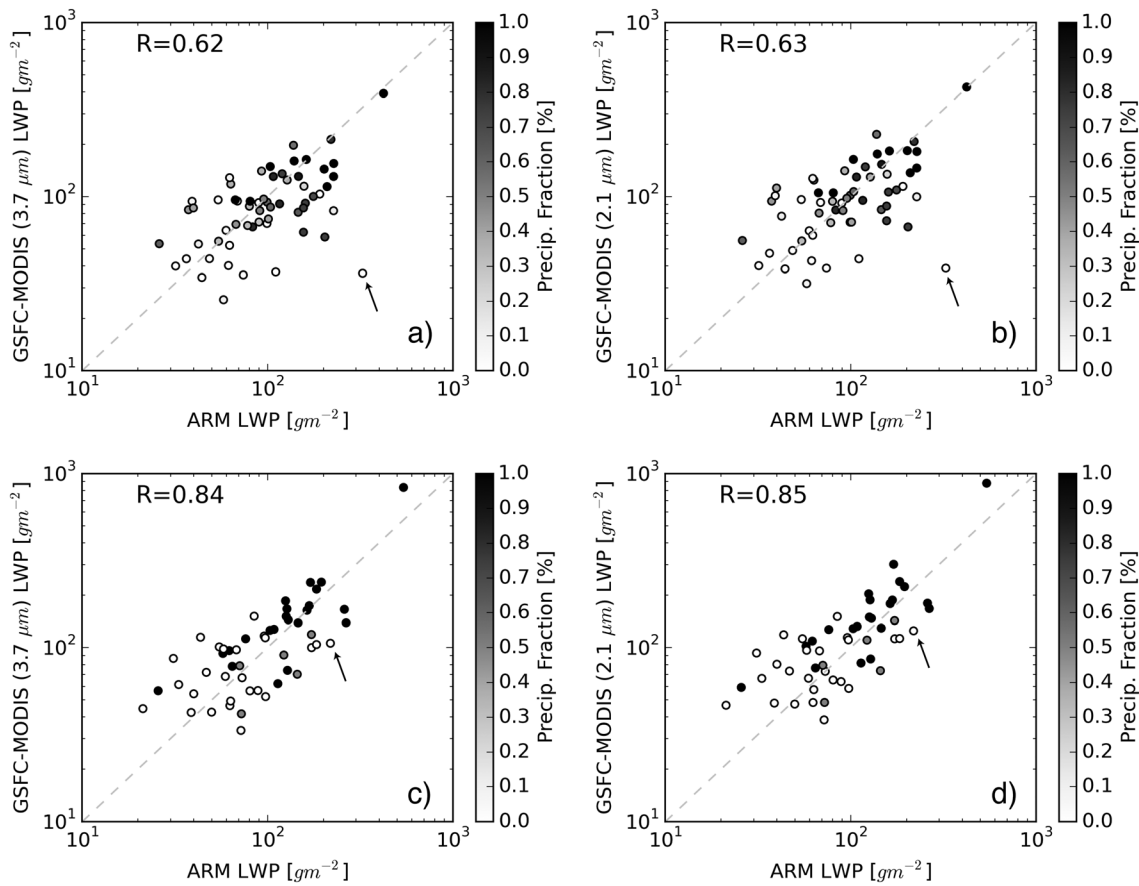


Figure 5. Comparisons of ground-based LWP retrievals from MWR with the GSFC-MODIS (a) LWP_{2,1} and (b) LWP_{3,7} products using the dL30km-dt60min averaging scheme. (c and d) Same as Figures 5a and 5b except for the averages from the dL10km-dt10min scheme. Gray scale of the dots corresponds to the fraction of precipitating MBL clouds during the temporal averaging window according to the ARM ground-based MMCR observations. The small arrow in the figure marks the 14 May 2010 case (see Figure 6 and text for details).

based on the MMCR observations. A case with darker color indicates a larger fraction of MBL clouds observed by the MWR during the temporal averaging window are precipitating. As expected, the cases with larger precipitation fraction (i.e., darker dots) generally have larger mean LWPs than those with mostly nonprecipitating clouds. Interestingly, the comparison between ground-based and GSFC-MODIS LWP retrievals shows no apparent dependence on the precipitation fraction because the light drizzle cases used in Xi14 to have little impact on the LWP retrievals. Further investigation is needed to better understand the impacts of drizzle on the MWR and MODIS retrievals and their differences.

Given the LWP comparisons, we now compare COT and CER values. Figure 7 shows comparisons of the GSFC-MODIS COT, CER_{2,1} and CER_{3,7} values with their ground-based counterparts based on the *Dong et al.* [1998] parameterization described in section 2.1.2. As in Figure 5, the gray scale in Figure 7 indicates the fraction of precipitation during the temporal averaging window based on the MMCR observations. When the dL30km-dt60min averaging scheme is used, the correlation coefficient between ground- and satellite-based COT retrievals for the 63 Xi14 cases is 0.62, which is consistent with the CERES-MODIS results

Table 1. Correlation Coefficient Between Ground-Based LWP Retrievals From MWR and Satellite-Based LWP Retrievals From GSFC-MODIS Product for Different Collocation Strategies

	dL = 30 km	dL = 20 km	dL = 10 km
dt = 60 min	0.62 (0.63)	0.66 (0.67)	0.71 (0.73)
dt = 30 min	0.66 (0.67)	0.72 (0.73)	0.77 (0.78)
dt = 10 min	0.75 (0.75)	0.79 (0.79)	0.84 (0.85)

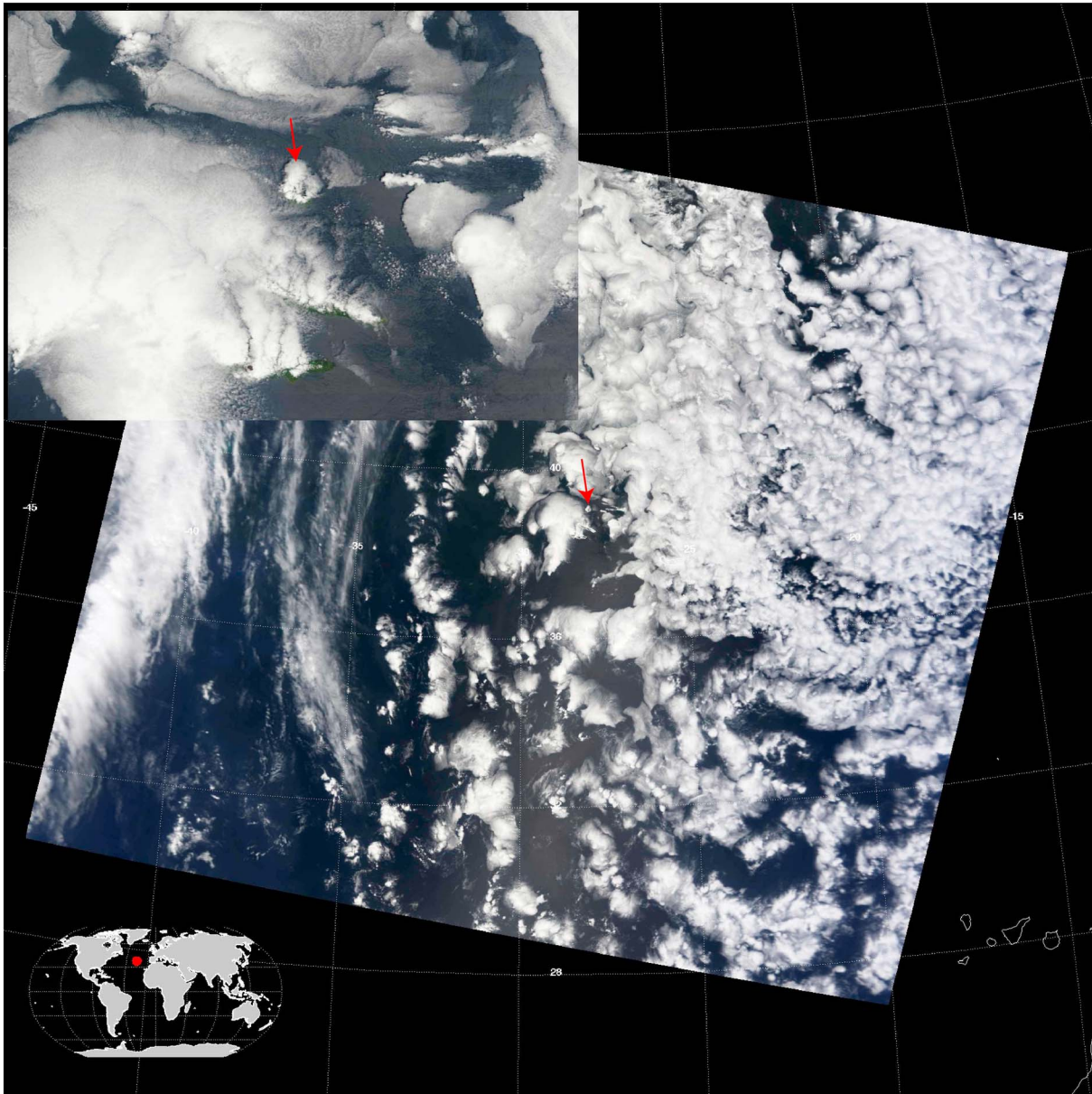


Figure 6. The RGB image from Terra-MODIS for the 14 May 2010 case. The red arrow indicates the island of Graciosa (39.09°N, 28.03°W) where the ARM AMF is located.

in Xi14 and also comparable to the correlation coefficient for LWP in Figures 5a and 5b. The ARM retrievals seem to be systematically higher than the GSFC-MODIS COT retrievals, as found in Xi14. Indeed, the P value based on the t test is only 0.04 for the null hypothesis test that the two COT data sets have the same mean value. When the averaging window is reduced to dL10km-dt10min, the correlation coefficient for COT increases slightly to 0.7, which is encouraging but not as significant as that seen in Figure 5 for LWP. The P value also increases to 0.89, indicating that smaller averaging window helps to reduce the bias. The CER comparisons between the GSFC-MODIS and ARM retrievals using the dL10km-dt10min scheme, on the other hand, have nearly the same correlations as those using the dL30km-dt60min averaging scheme but larger mean differences and standard deviations. The LWP, COT, and CER comparisons have demonstrated that the dL10km-dt10min scheme can increase the correlation but does not always diminish the satellite-surface differences as shown in Dong *et al.* [2008]. This is primarily due to mismatch between the surface temporal averages and satellite spatial averages and uncertainties in the two retrieval methods.

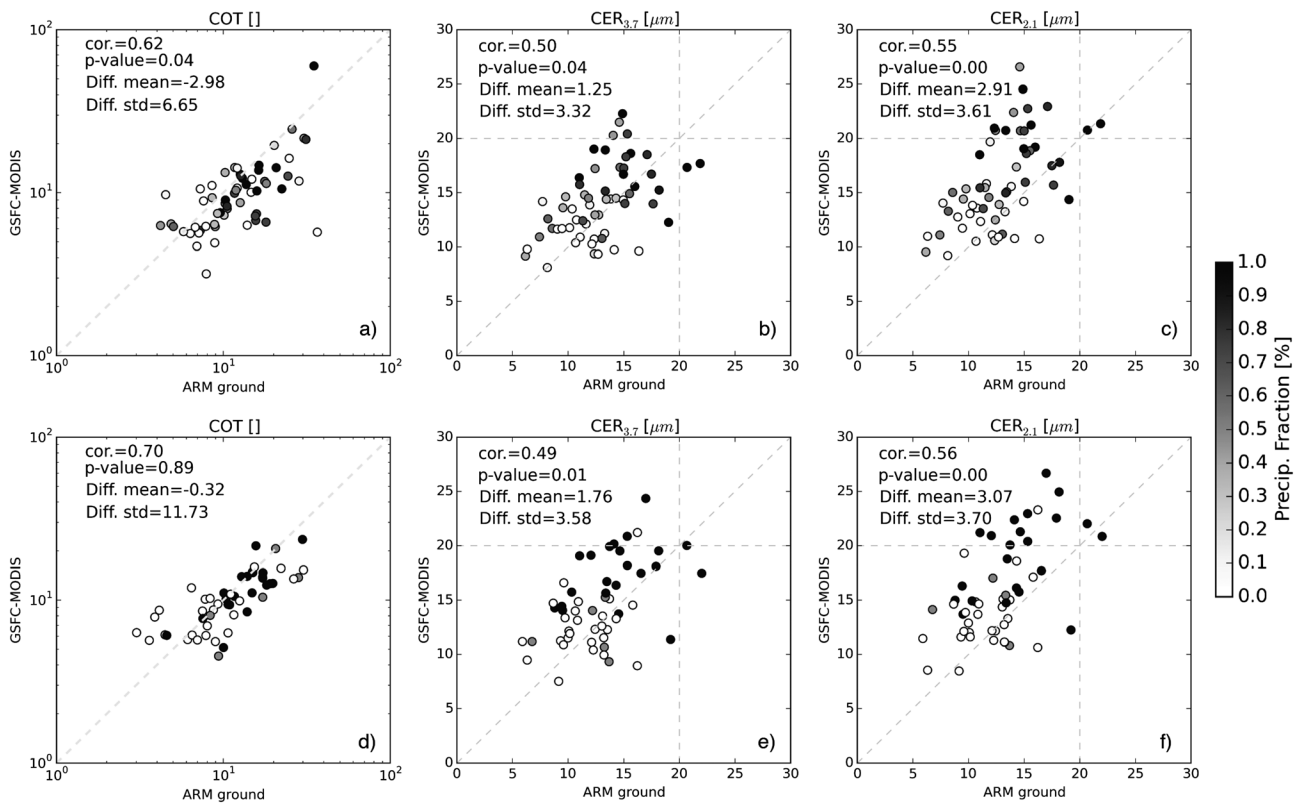


Figure 7. Comparisons of (a) COT, (b) $CER_{2.1}$, and (c) $CER_{3.7}$ from GSFC-MODIS cloud product with the ground-based retrievals based on *Dong et al.* [1998] algorithm under the dL30km-dt60min averaging scheme. (d–f) Same as Figures 7a–7c expect for averaging based on dL10km-dt10min scheme.

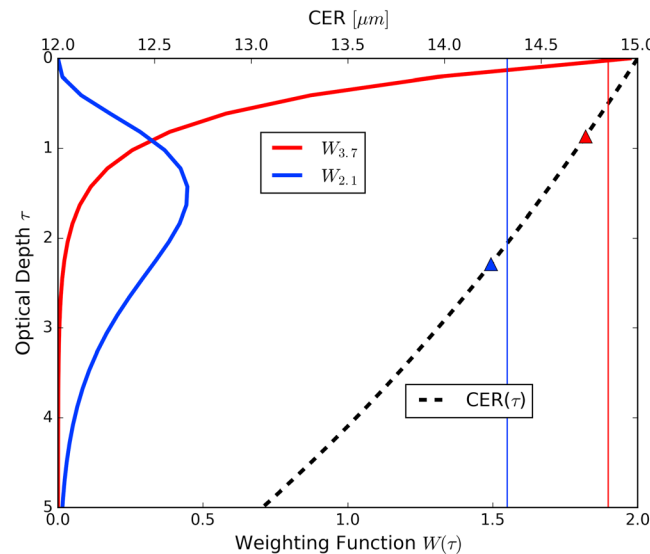


Figure 8. Schematic diagram to illustrate the vertical distributions of CER and COT from two MODIS bands. The red and blue solid curves are the weighted COTs $W(\tau)$ for $CER_{3.7}$ and $CER_{2.1}$ retrievals, respectively. The dashed black curve corresponds to an adiabatic CER profile with the $CER = 15 \mu m$ at cloud top. The red and blue triangles mark the $CER_{3.7}$ and $CER_{2.1}$ retrievals from theoretical calculations. The red and blue vertical lines mark the locations of the retrieved $CER_{3.7}$ and $CER_{2.1}$ predicted by the weighting function in equation (4). In this case $\mu = \mu_0 = 1$, the total COT = 10, and the CER profile follows the classic adiabatic structure.

Figure 7 also compares the GSFC-MODIS $CER_{2.1}$ and $CER_{3.7}$ retrievals with the *Dong et al.* [1998] ground-based CER retrievals. When the dL30km-dt60min averaging scheme is used, the correlation coefficient for $CER_{3.7}$ and $CER_{2.1}$ is 0.50 (Figure 7b) and 0.55 (Figure 7c), respectively. More importantly, based on the average of the 63 cases, $CER_{3.7}$ and $CER_{2.1}$ are 1.3 and 2.9 μm larger, respectively, than the *Dong et al.* [1998] ground-based CER averages, indicating the existence of systematic bias. Unlike the LWP and COT comparisons, the comparison of CER does not show any significant improvement when the averaging window drops to dL10km-dt10min (Figures 7e and 7f). The correlation coefficient remains low around 0.5 and the bias even increases slightly.

In contrast to column-integrated variables like LWP and COT, CER is dependent on the vertical structure of MBL clouds. As mentioned in section 2, the

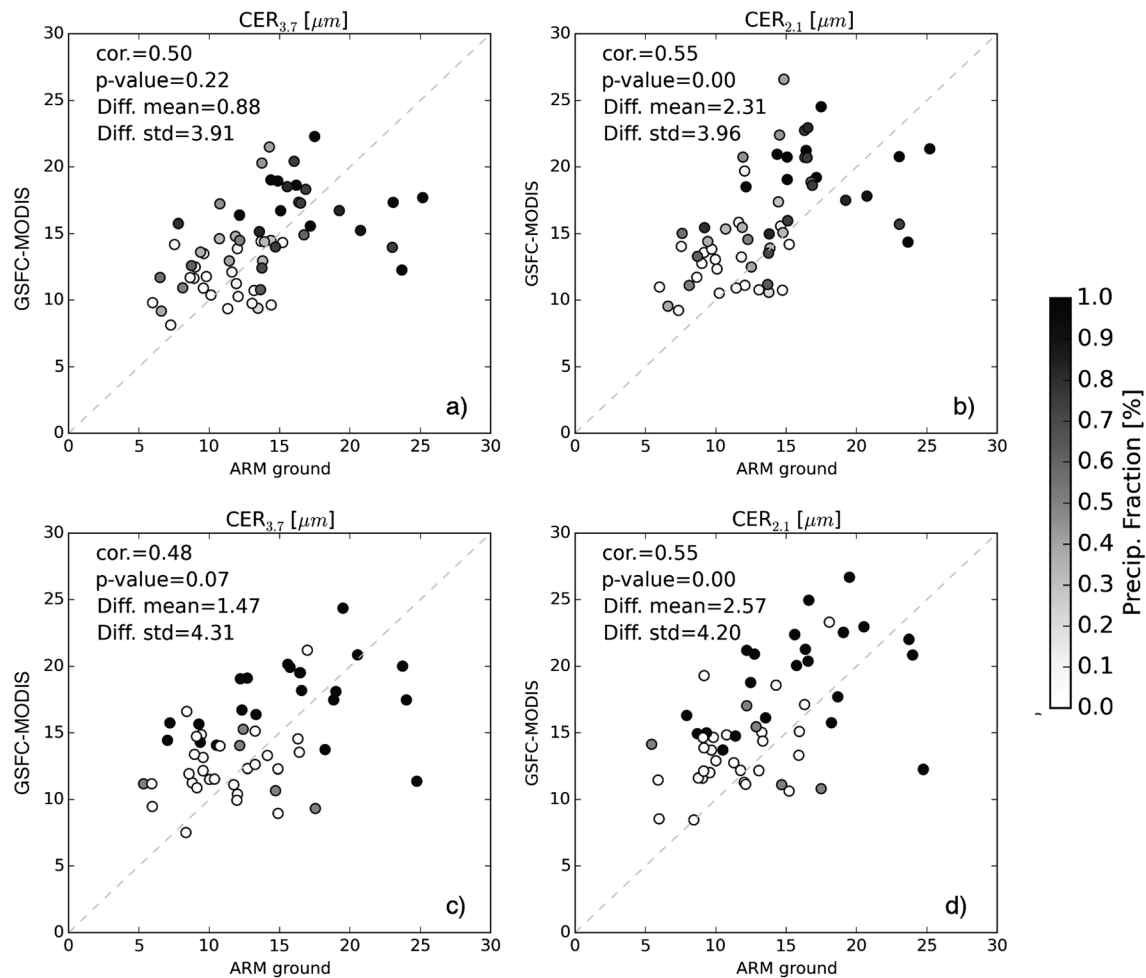


Figure 9. Same as Figure 7, except that the ground-based CER retrievals are vertically weighted results using the analytical weighing function in equation (4) and the LWC and CER profile from *Dong and Mace* [2010] algorithm.

MODIS CER retrievals are only sensitive to the upper portion of the MBL clouds, while the ground-based CER retrievals from *Dong et al.* [1998] can be considered as the vertical average of the CER profile. Could this be the primary reason causing the differences between ground- and satellite-based CER retrievals seen in Figure 7? The ground-based CER and LWC profile retrievals from *Dong and Mace* [2010] provide the observations needed to address this question. To illustrate and quantify the sensitivity of MODIS CER retrieval to cloud vertical structure, *Platnick* [2000] introduced the concept of a vertical weighting function $W(\tau)$, which relates the MODIS CER retrieval with the vertical profile of CER as follows:

$$CER^* = \int_0^{COT} CER(\tau)W(\tau)d\tau, \tag{3}$$

where τ is the optical depth from cloud top and $CER(\tau)$ is the CER profile as a function of τ . $W(\tau)$ is normalized so that $\int_0^{COT} W(\tau)d\tau = 1$. Given a CER profile, the computation of $W(\tau)$ involves rather expensive radiative transfer simulations. In this study, we adopt the concept of the vertical weighting function but use an analytical form that can serve as a first-order approximation to the actual weighting function to avoid expensive radiative transfer simulations:

$$W(\tau) = a\tau^b \exp\left[-\tau\left(\frac{1}{\mu} + \frac{1}{\mu_0}\right)\right], \tag{4}$$

where μ and μ_0 are the cosines of viewing and solar zenith angles, respectively, the exponent b determines the location of the maximum sensitivity, and a is a constant to ensure that $W(\tau)$ is normalized. Because of the stronger cloud absorption in the 3.7 μm band, we let $b=0$ to approximately reduce $W(\tau)$ to the two-way

transmittance [Alexandrov *et al.*, 2012; Miller *et al.*, 2016]. Meanwhile, we use $b=2$ for the $CER_{2,1}$ to allow a deeper penetration depth. A hypothetical example to demonstrate the use of the analytical weighting function is given in Figure 8. For this particular case, the $CER_{3,7}$ and $CER_{2,1}$ retrieval results predicted based on our analytical $W(\tau)$ are in reasonable agreement with the numerical simulations, although biased a little higher, lending confidence to our analytical $W(\tau)$ in equation (4).

To account for the sensitivity of the MODIS CER retrievals to cloud vertical structure in the comparison, we first use the LWC and CER profiles from the Dong and Mace [2010] scheme that are described in section 2.1.3 to derive the vertical profile of CER as a function of optical depth, i.e., $CER(\tau)$. Then, we use the analytical $W(\tau)$ to derive from equation (3) what the MODIS $CER_{3,7}$ and $CER_{2,1}$ retrieval results would be if the MODIS instrument had observed a MBL cloud with the given LWC and CER profiles (referred to as the “ARM vertically weighted” retrievals). Finally, we compare the ARM vertically weighted CER with the GSFC-MODIS retrievals in Figure 9. In comparison to the results in Figure 7, the vertical weighting helps to reduce the MODIS CER bias by $\sim 0.5 \mu\text{m}$ for both dL30km-dt60min and dL10km-dt10min averaging schemes. These results are consistent with the theoretical expectation. Nonetheless, there are still significant differences between ground- and satellite-based results. Depending on which averaging scheme is used, the GSFC-MODIS $CER_{3,7}$ retrievals for the 63 Xi14 cases are about 0.9 to 1.5 μm larger than the ground-based CER retrievals, even if the MODIS CER retrieval sensitivity to the cloud vertical structure is considered. The $CER_{2,1}$ retrievals are even larger (by about 2.3 to 2.6 μm).

4. Conclusions and Discussion

The DOE ARM Program carried out a 19 month observation field campaign from April 2009 to December 2010—the CAP-MBL—on Graciosa Island (39° 5′ 28″ N, 28° 1′ 45″ W), targeting MBL clouds over the Azores. Here we present an intercomparison of the MBL cloud LWP, COT, and CER between the CAP-MBL ARM AMF retrievals and two satellite remote sensing products (CERES-MODIS and GSFC-MODIS). The main results from the comparison are summarized as follows:

1. The two MODIS products show good agreement on COT and $CER_{3,7}$ (correlation coefficient $R \sim 0.95$). The $CER_{2,1}$ from CERES-MODIS product is systematically larger than that from GSFC-MODIS possibly due to calibration and/or algorithmic differences. In both MODIS products, MBL $CER_{2,1}$ tends to be larger than $CER_{3,7}$. The magnitude of $CER_{2,1} - CER_{3,7}$ increases with cloud subpixel inhomogeneity, suggesting that the plane-parallel homogeneous bias likely plays an important role in the spectral retrieval differences.
2. Comparison between the ARM ground-based cloud retrievals and the GSFC-MODIS product depends on how the two data sets are collocated. A more precise collocation generally leads to better agreement. We found no systematic bias between the ground-based MWR and GSFC-MODIS LWP values. The correlation coefficient is about 0.85 for the 63 selected cases when using a more strict collocation scheme (dL10km-dt10min), while R reduces to 0.62 when using a more relaxed collocation scheme (dL30km-dt60min). Similarly, the ground- and satellite-based COT retrievals also agree reasonably well, with no apparent bias and correlation coefficient $R \sim 0.70$.
3. Averaging over the 63 selected cases, the GSFC-MODIS $CER_{2,1}$ and $CER_{3,7}$ are about 1.5 μm and 3.0 μm larger than ground-based retrievals based on the Dong *et al.* [1998] scheme. Taking into account that the satellite-based CER retrievals are only sensitive to cloud top reduces this bias by $\sim 0.5 \mu\text{m}$. Precipitation seems to have little impact on the comparison.

These findings have several implications. First, the good agreement on instantaneous MODIS retrievals should lend confidence to both MODIS products. They can be deemed to be practically equivalent for studying the climatology of MBL clouds or evaluating the MBL cloud simulations in GCMs. The fact that $CER_{2,1}$ is systematically larger than $CER_{3,7}$ in both MODIS products indicates this spectral difference unlikely to be an algorithm issue but caused by more fundamental issues like subpixel level cloud inhomogeneity. Second, in comparison with Xi14, a more precise temporal-spatial collocation in this study leads to a better agreement between ground- and satellite-based retrievals of LWP and COT. Together, the ARM and MODIS cloud property retrievals constitute a strong constraint on the bulk physical and optical properties of MBL clouds over the Azores region that should be highly useful for GCM evaluation. Finally, the differences between the ground- and satellite-based CER indicate the existence of significant uncertainty in the current observations of MBL cloud microphysics. Although the cause is yet to be understood, this study provides a

quantitative assessment of this uncertainty, which could still be helpful for evaluating the GCM simulations of MBL clouds. This study is based on limited cases. Now the ARM program has established a permanent site on the Graciosa Island for long-term observations. We will extend our comparisons to the new data record in future studies.

Acknowledgments

This research is supported by Department of Energy (DOE) Regional & Global Climate Modeling Program (grant DE-SC0014641) managed by Renu Joseph. The computations in this study were performed at the UMBC High Performance Computing Facility (HPCF). The facility is supported by the U.S. National Science Foundation through the MRI program (grants CNS-0821258 and CNS-1228778) and the SCREMS program (grant DMS-0821311), with additional substantial support from UMBC. The ground-based retrievals and measurements from the DOE CAP-MBL campaign are available from DOE ARM data server <http://www.archive.arm.gov/armlogin/login.jsp>. The MODIS data are obtained from NASA's Level 1 and Atmosphere Archive and Distribution System (LAADS <http://ladsweb.nascom.nasa.gov/>).

References

- Alexandrov, M. D., B. Cairns, C. Emde, A. S. Ackerman, and B. van Diedenhoven (2012), Accuracy assessments of cloud droplet size retrievals from polarized reflectance measurements by the research scanning polarimeter, *Remote Sens. Environ.*, *125*(0), 92–111, doi:10.1016/j.rse.2012.07.012.
- Dolarin, E. K., X. Dong, B. Xi, J. H. Jiang, and H. Su (2014), Evaluation of CMIP5 simulated clouds and TOA radiation budgets using NASA satellite observations, *Clim. Dyn.*, *44*(7–8), 2229–2247, doi:10.1007/s00382-014-2158-9.
- Dong, X., and G. G. Mace (2010), Profiles of low-level stratus cloud microphysics deduced from ground-based measurements, *J. Atmos. Oceanic Technol.*, *20*(1), 42–53, doi:10.1175/1520-0426(2003)020<0042:POLLSC>2.0.CO;2.
- Dong, X., T. P. Ackerman, E. E. Clothiaux, P. Pilewskie, and Y. Han (1997), Microphysical and radiative properties of boundary layer stratiform clouds deduced from ground-based measurements, *J. Geophys. Res.*, *102*(D20), 23,829–23,843, doi:10.1029/97JD02119.
- Dong, X., T. P. Ackerman, and E. E. Clothiaux (1998), Parameterizations of the microphysical and shortwave radiative properties of boundary layer stratus from ground-based measurements, *J. Geophys. Res.*, *103*(D24), 31,681–31,693, doi:10.1029/1998JD200047.
- Dong, X., P. Minnis, B. Xi, S. Sun Mack, and Y. Chen (2008), Comparison of CERES-MODIS stratus cloud properties with ground-based measurements at the DOE ARM Southern Great Plains site, *J. Geophys. Res.*, *113*, D03204, doi:10.1029/2007JD008438.
- Dong, X., B. Xi, A. Kennedy, P. Minnis, and R. Wood (2014a), A 19-month record of marine aerosol–cloud–radiation properties derived from DOE ARM mobile facility deployment at the Azores. Part I: Cloud fraction and single-layered MBL cloud properties, *J. Clim.*, *27*(10), 3665–3682, doi:10.1175/JCLI-D-13-00553.1.
- Dong, X., B. Xi, and P. Wu (2014b), Investigation of the diurnal variation of marine boundary layer cloud microphysical properties at the Azores, *J. Clim.*, *27*(23), 8827–8835, doi:10.1175/JCLI-D-14-00434.1.
- Kay, J. E., et al. (2012), Exposing global cloud biases in the Community Atmosphere Model (CAM) using satellite observations and their corresponding instrument simulators, *J. Clim.*, *25*(15), 5190–5207, doi:10.1175/JCLI-D-11-00469.1.
- Klein, S., and D. Hartmann (1993), The seasonal cycle of low stratiform clouds, *J. Clim.*, *6*(8), 1587–1606.
- Lebsock, M., and H. Su (2014), Application of active spaceborne remote sensing for understanding biases between passive cloud water path retrievals, *J. Geophys. Res. Atmos.*, *119*, 8962–8979, doi:10.1002/2014JD021568.
- Lebsock, M. D., and T. S. L'Ecuyer (2011), The retrieval of warm rain from CloudSat, *J. Geophys. Res.*, *116*, D20209, doi:10.1029/2011JD016076.
- Lebsock, M. D., T. S. L'Ecuyer, and G. L. Stephens (2011), Detecting the ratio of rain and cloud water in low-latitude shallow marine clouds, *J. Appl. Meteorol. Climatol.*, *50*(2), 419–432, doi:10.1175/2010JAMC2494.1.
- Liljegren, J. C., E. E. Clothiaux, G. G. Mace, S. Kato, and X. Dong (2001), A new retrieval for cloud liquid water path using a ground-based microwave radiometer and measurements of cloud temperature, *J. Geophys. Res.*, *106*(D13), 14,485–14,500, doi:10.1029/2000JD900817.
- Loeb, N. G., S. Kato, K. Loukachine, and N. Manalo-Smith (2005), Angular distribution models for top-of-atmosphere radiative flux estimation from the clouds and the Earth's radiant energy system instrument on the Terra satellite. Part I: Methodology, *J. Atmos. Oceanic Technol.*, *22*(4), 338–351, doi:10.1175/JTECH1712.1.
- Logan, T., B. Xi, and X. Dong (2014), Aerosol properties and their influences on marine boundary layer cloud condensation nuclei at the ARM mobile facility over the Azores, *J. Geophys. Res. Atmos.*, *119*, 4859–4872, doi:10.1002/2013JD021288.
- Long, C. N., and T. P. Ackerman (2000), Identification of clear skies from broadband pyranometer measurements and calculation of downwelling shortwave cloud effects, *J. Geophys. Res.*, *105*(D12), 15,609–15,626, doi:10.1029/2000JD900077.
- Miller, D. J., Z. Zhang, A. S. Ackerman, S. Platnick, and B. A. Baum (2016), The impact of cloud vertical profile on liquid water path retrieval based on the bispectral method: A theoretical study based on large-eddy simulations of shallow marine boundary layer clouds, *J. Geophys. Res. Atmos.*, *121*, 4122–4141, doi:10.1002/2015JD024322.
- Minnis, P., R. Arduini, D. Young, and J. Ayers (2004), An examination of the impact of drizzle drops on satellite-retrieved effective particle sizes... of 14th International Conference on Clouds and
- Minnis, P., et al. (2011a), CERES Edition-2 cloud property retrievals using TRMM VIRS and Terra and Aqua MODIS data—Part II: Examples of average results and comparisons with other data, *IEEE Trans. Geosci. Remote Sens.*, *49*(11), 4401–4430, doi:10.1109/TGRS.2011.2144602.
- Minnis, P., et al. (2011b), CERES Edition-2 cloud property retrievals using TRMM VIRS and Terra and Aqua MODIS data—Part I: Algorithms, *IEEE Trans. Geosci. Remote Sens.*, *49*(11), 4374–4400, doi:10.1109/TGRS.2011.2144601.
- Minnis, P., S. Sun-Mack, Y. Chen, M. M. Khaiyer, Y. Yi, J. K. Ayers, R. R. Brown, X. Dong, S. C. Gibson, and P. W. Heck (2011c), CERES Edition-2 cloud property retrievals using TRMM VIRS and Terra and Aqua MODIS data—Part II: Examples of average results and comparisons with other data, *IEEE Trans. Geosci. Remote Sens.*, *49*(11), 4401–4430.
- Nakajima, T., M. D. King, and J. D. Spinhirne (1990), Determination of the optical thickness and effective particle radius of clouds from reflected solar radiation measurements. Part I: Theory, *JAS*, *47*(15), 1878–1893, doi:10.1175/1520-0469(1990)047<1878:DOTOTA>2.0.CO;2.
- Nakajima, T. Y., K. Suzuki, and G. L. Stephens (2010), Droplet growth in warm water clouds observed by the A-Train. Part I: Sensitivity analysis of the MODIS-derived cloud droplet sizes, *J. Atmos. Sci.*, *67*(6), 1884–1896, doi:10.1175/2009JAS3280.1.
- Painemal, D., and P. Zuidema (2011), Assessment of MODIS cloud effective radius and optical thickness retrievals over the Southeast Pacific with VOCALS-REx in situ measurements, *J. Geophys. Res.*, *116*, D24206, doi:10.1029/2011JD016155.
- Painemal, D., P. Minnis, J. K. Ayers, and L. O'Neill (2012), GOES-10 microphysical retrievals in marine warm clouds: Multi-instrument validation and daytime cycle over the southeast Pacific, *J. Geophys. Res.*, *117*, D19212, doi:10.1029/2012JD017822.
- Painemal, D., P. Minnis, and S. Sun-Mack (2013), The impact of horizontal heterogeneities, cloud fraction, and liquid water path on warm cloud effective radii from CERES-like Aqua MODIS retrievals, *ACP*, *13*(19), 9997–10,003, doi:10.5194/acpd-13-12725-2013.
- Pincus, R., S. Platnick, S. A. Ackerman, R. S. Hemler, and R. J. Patrick Hofmann (2012), Reconciling simulated and observed views of clouds: MODIS, ISCCP, and the limits of instrument simulators, *J. Clim.*, *25*, 120220120058001, doi:10.1175/JCLI-D-11-00267.1.
- Platnick, S. (2000), Vertical photon transport in cloud remote sensing problems, *J. Geophys. Res.*, *105*(D18), 22,919–22,935, doi:10.1029/2000JD900333.

- Platnick, S., M. D. King, S. A. Ackerman, W. P. Menzel, B. A. Baum, J. C. Riédi, and R. A. Frey (2003), The MODIS cloud products: Algorithms and examples from Terra, *IEEE Trans. Geosci. Remote Sens.*, *41*(2), 459–473, doi:10.1109/TGRS.2002.808301.
- Platnick, S., et al. (2016), The MODIS cloud optical and microphysical products: Collection 6 updates and examples from Terra and Aqua, *IEEE Trans. Geosci. Remote Sens.*, *55*(1), 502–525, doi:10.1109/TGRS.2016.2610522, "rightsLink": "http://s100.copyright.com/AppDispatchServlet?publisherName=ieee&publication=0196-2892&title=The+MODIS+Cloud+Optical+and+Microphysical+Products%3A+Collection+6+Updates+and+Examples+From+Terra+and+Aqua&isbn=&publicationDate=Jan.+2017&author=Steven+Platnick&ContentID=10.1109/TGRS.2016.2610522&orderBeanReset=true&startPage=502&endPage=525&volumeNum=55&issueNum=1", "displayPublicationTitle": "IEEE.
- Seethala, C., and Á. Horváth (2010), Global assessment of AMSR-E and MODIS cloud liquid water path retrievals in warm oceanic clouds, *J. Geophys. Res.*, *115*, D13202, doi:10.1029/2009JD012662.
- Wood, R. (2012), Stratocumulus Clouds, *Mon. Weather Rev.*, *140*(8), 2373–2423, doi:10.1175/MWR-D-11-00121.1.
- Wood, R., et al. (2015), Clouds, Aerosols, and Precipitation in the Marine Boundary Layer: An Arm Mobile Facility Deployment, *Bull. Am. Meteorol. Soc.*, *96*(3), 419–440, doi:10.1175/BAMS-D-13-00180.1.
- Xi, B., X. Dong, P. Minnis, and S. Sun Mack (2014), Comparison of marine boundary layer cloud properties from CERES-MODIS Edition 4 and DOE ARM AMF measurements at the Azores, *J. Geophys. Res.-Atmos.*, *119*, 9509–9529, doi:10.1002/2014JD021813.
- Zhang, Z., and S. Platnick (2011), An assessment of differences between cloud effective particle radius retrievals for marine water clouds from three MODIS spectral bands, *J. Geophys. Res.*, *116*, D20215, doi:10.1029/2011JD016216.
- Zhang, Z., A. S. Ackerman, G. Feingold, S. Platnick, R. Pincus, and H. Xue (2012), Effects of cloud horizontal inhomogeneity and drizzle on remote sensing of cloud droplet effective radius: Case studies based on large-eddy simulations, *J. Geophys. Res.*, *117*, D19208, doi:10.1029/2012JD017655.